

# The effect of dynamic bending moments on the ratchetting behavior of stainless steel pressurized piping elbows

S. J. Zakavi, V. Golshan\*

Faculty of Mech.Eng, Uni.of Mohaghegh Ardabili, Ardabil, Iran

## Email address:

zakavi@uma.ac.ir (S. J. Zakavi), Vahid.golshan@yahoo.com (V. Golshan)

## To cite this article:

S. J. Zakavi, V. Golshan. The Effect of Dynamic Bending Moments on the Ratchetting Behavior of Stainless Steel Pressurized Piping Elbows. *International Journal of Mechanical Engineering and Applications*. Vol. 2, No. 2, 2014, pp. 31-37.  
doi: 10.11648/j.ijmea.20140202.12

**Abstract:** In this paper the ratchetting behavior of four pairs of stainless steel, long and short radius welding elbows is studied under conditions of steady internal pressure and in-plane, resonant dynamic moments that simulated seismic excitations. The finite element analysis with the nonlinear kinematic hardening model has been used to evaluate ratchetting behavior of the elbow under mentioned loading condition. Stress-strain data and material parameters have been obtained from several stabilized cycles of specimens that are subjected to symmetric strain cycles. The results show that the maximum ratcheting strain occurred mainly in the hoop direction at flanks. Ratcheting strain rate increases with increase of the bending loading level at the constant internal pressure. The results show that the FE method gives over estimated values comparing with the experimental data.

**Keywords:** Ratchetting, Pressurized Elbows, Cyclic Bending Moment, Strain Hardening Model, Stainless Steel

## 1. Introduction

Ratchetting, namely the accumulation of plastic deformation, occurs when the structures are subjected to a primary load with a secondary cyclic load if the applied loads are high enough to make the structures yield. In the materials or structures subjected to a cyclic stressing with non-zero mean stress, a cyclic accumulation of inelastic deformation will occur if the applied stress is high enough which is called ratcheting. Plastic analysis of structures is usually studied using the isotropic and kinematic hardening theories. Ratcheting description in terms of the conventional equations is mainly related to kinematic hardening. Pressurized piping as the most basic structures in chemical industries and power plants are subjected to variable mechanical and thermal loads which often have a cyclic nature. Accurate determination of the plastic strain rate in each cycle is important subject in pressurized piping of power plant and chemical industries. Collapse, ratcheting, and fatigue interaction may occur and lead to failures. Thus, during the design of pressurized piping today, especially which used in chemical industries and power plant components, ratcheting and ratcheting fatigue must be under consideration.

The literature review shows that accurate closed form

solutions may not be found to analyse the ratchetting behavior of the pressurized pipes under cyclic bending loading which can be caused by seismic loads. However, approximate solutions have been developed by Tasnim et al. (1992, 2008), Rahman et al. (2008), Zakavi et al. (2010), Chaboche (1989,1991,2008), Chen et al. (2005,2006, 2013), Abdel-Karim (2005), Ohno et al. (1993), Bari and Hassan (2000,2001,2002) which can be used to calculate the induced incremental plastic strains caused by ratchetting. Experimental works to study the ratchetting of the elbow pipes have also been carried out by Chen et al. (2013) and Yahiaoui et al., (1996).

## 2. Materials and Methods

In this paper, a finite element code, ABAQUS, is used to study the ratchetting of stainless steel pressurized elbow subjected to cyclic bending loading. In the experimental tests (Yahiaoui et al., 1996), series of tests have been undertaken subjecting pressurized elbow specimens to rising amplitude dynamic (5 Hz, the resonant frequency) bending moments. Then, by conducting a series of finite element runs based on the nonlinear kinematic hardening model using the ABAQUS, the experimental tests are modeled and ratchetting data obtained. Then the two sets of results are

compared with each other.

### 3. Nonlinear Kinematic Hardening Models

The kinematic hardening models are used to simulate the inelastic behavior of materials that are subjected to cyclic loading. The use of plasticity material models with isotropic type hardening is generally not recommended since they continue to harden during cyclic loading. The isotropic hardening model always predicts shakedown behavior, if creep is not considered (Mahbadi et al., 2006). The kinematic hardening plasticity models are proposed to model the inelastic behavior of materials that are subjected to repeated loading. For example, the Armstrong-Frederick (1996) kinematic hardening model is suggested for the nonlinear strain hardening materials.

Based on the Armstrong-Frederick nonlinear kinematic hardening rule, many constitutive models have been constructed to simulate the uniaxial and multiaxial ratchetting of materials characterized by cyclic hardening or cyclic stable behaviors. The results of these models are discussed for structures under various types of cyclic loads in references.

The classical linear kinematic hardening rule and different nonlinear kinematic hardening models are available for the plastic analysis of structures. The nonlinear kinematic hardening model was first proposed by Armstrong and Frederick (1996). Nonlinearities are given as a recall term in the Prager rule. So that the transformation of yield surface in the stress space is different during loading and unloading. This is done by assuming different hardening modulus in loading and unloading conditions. The yield function for time independent plasticity, using the von-Mises yield criterion, is expressed as (Lemaitre and Chaboche, 1994):

$$f = J_2(\sigma - X) - k \quad (1)$$

where  $X$  is the back stress tensor,  $k$  the initial size of the yield surface, and denotes the von-Mises distance in the deviatoric stress space:

$$J_2(\sigma - X) = \left[ \left( \frac{3}{2} \sigma' - X' \right) : (\sigma' - X') \right]^{\frac{1}{2}} \quad (2)$$

where  $\sigma$  and  $X$  are the stress and back stress tensors, and  $\sigma'$  and  $X'$  are the stress and back stress deviatoric tensors in the stress space, respectively. The nonlinearities are given as a recall term in the Prager rule:

$$dX = \frac{2}{3} C d\varepsilon_p - \gamma X d\varepsilon_p \quad (3)$$

where  $d\varepsilon_p$  is the equivalent plastic strain rate,  $C$  and  $\gamma$  are two material dependent coefficients in the Armstrong-Frederick kinematic hardening model, and

$\gamma = 0$  stands for the linear kinematic rule. The normality hypothesis and the consistency condition  $df = 0$  lead to the expression for the plastic strain rate (Lemaitre and Chaboche, 1994):

$$d\varepsilon^p = d \frac{\partial f}{\partial \sigma} = \frac{H(f)}{h} \left\langle \frac{\partial f}{\partial \sigma} : d\sigma \right\rangle \frac{\partial f}{\partial \sigma} \quad (4)$$

where  $H$  denotes the Heaviside step function:  $H(f) = 0$  if  $f < 0$ ,  $H(f) = 1$  if  $f \geq 0$  and the symbol  $\langle \rangle$  denotes the MacCauley bracket, i.e.,  $\langle u \rangle = (u + |u|)/2$ . The hardening modulus  $h$  becomes:

$$h = C - \frac{3}{2} \gamma X : \frac{\sigma' - X'}{k} \quad (5)$$

In the case of tension-compression, the criterion and the equations of flow and hardening can be expressed in the form (Lemaitre and Chaboche, 1994):

$$f = |\sigma - X| - k = 0 \quad (6)$$

$$d\varepsilon_p = \frac{1}{h} \left\langle \frac{\sigma - X}{k} d\sigma \right\rangle \frac{\sigma - X}{k} = \frac{d\sigma}{h} \quad (7)$$

$$dX = C d\varepsilon_p - \gamma X |d\varepsilon_p| \quad (8)$$

$$h = C - \gamma X \text{Sgn}(\sigma - X) \quad (9)$$

The evolution equation of hardening can be integrated analytically to give:

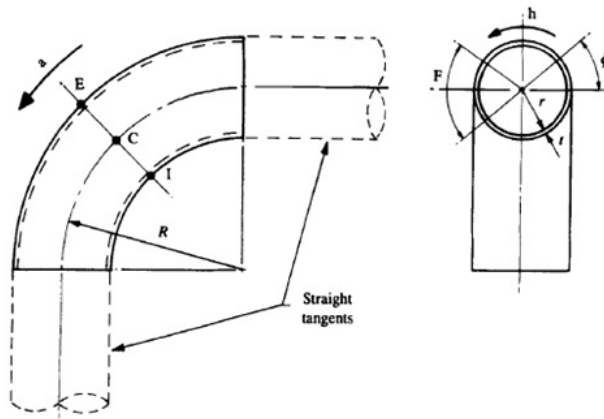
$$X = \nu \frac{C}{\gamma} + \left( X_0 - \nu \frac{C}{\gamma} \right) \exp[-\nu \gamma (\varepsilon_p - \varepsilon_{p_0})] \quad (10)$$

where  $\nu = \pm 1$  according to the direction of flow, and  $\varepsilon_{p_0}$  and  $X_0$  are the initial values. For example at the beginning of each plastic flow.

### 4. Review of Experimental Set-Up (Yahiaoui et al., 1996)

The experimental set-up for testing piping elbows under in-plane bending has been reported in reference (Yahiaoui et al., 1996). The nominal pipe size was 2 inch NPS corresponding to an outside diameter of 60.3 mm. Elbow geometry and the parameters and section of the results is shown in Fig. 1. The component identification and relevant dimensions of the elbows are given in Table 1. Typical stress-strain curves for the stainless steel materials (304L) are shown in Fig. 2. For stainless steel (SS304) material, specification and properties obtained by tensile tests data is

given in Table 2. Pairs of 90° welding elbows were, for symmetry, tested simultaneously. The test components were pressurized independently to their design pressure, calculated using the ASME Code formula. The internal pressure was closely monitored and kept constant during testing. The frequency and design pressure of elbows is given in Table 3. Hoop strains at the crown reading from the gauges attached to the elbows at the crown positions (Fig. 1).



a = axial direction  
h = hoop direction  
 $\phi$  = angular position around mid-circumference section containing E, C and I = 0° at C and positive towards E  
C = crown positions ( $\phi = 0^\circ, 180^\circ$ )  
E = extrados ( $\phi = +90^\circ$ )  
F = flank regions (defined by  $\phi = \pm 45^\circ$  about the crowns)  
I = intrados ( $\phi = -90^\circ$ )

**Fig 1.** Elbow geometry, stress directions, angular coordinate and definition of important locations around the bend (Yahiaoui et al., 1996).

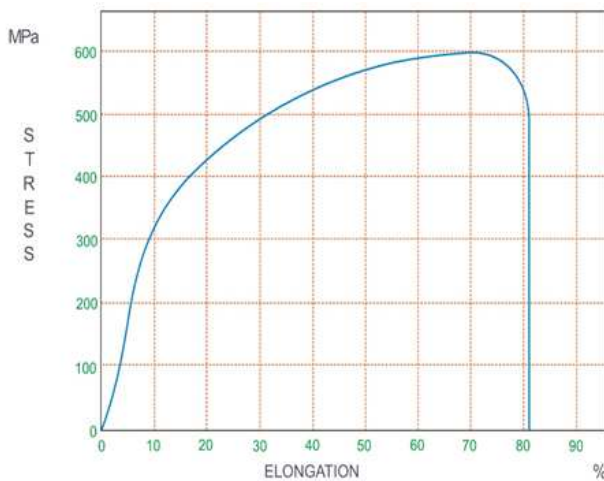


**Fig 2.** Stainless steel used to manufacture the tubular specimens.

## 5. Finite Element Arrangement

For all specimens the finite element code, ABAQUS, was used to study ratcheting behavior of pressurized elbows under simulated seismic bending moments. The elbows have a 1.50 m long pipework modeled by 28 elements. The most

accurate element in the ABAQUS code for this type of structural system considering beam elements, pipe elements and elbow elements is the elbow element. Four types of elbow elements are available in the ABAQUS library, of which the two-noded element ELBOW31 was found to give the best results. ELBOW31 provides accurate predictions of the behavior of elbows under monotonic loading. In this paper, in order to predict the results, the tensile specimens were produced accordance with the materials properties that is given in Table 2.

The cyclic nonlinear constitutive model used in the FEM analyses in this study is derived from multiaxial formulations by Armstrong and Frederick. It is recommended that the model be calibrated with experimental data that is close to the expected strain range and loading history of the application. Stress-strain data is obtained from several stabilized cycles of specimens that are subjected to symmetric strain cycles. The material parameters  $C$  and  $\gamma$  determine the kinematic hardening component of the model. Three different ways of providing data for the kinematic hardening component of the mode can be given: using half-cycle test data, using single stabilized cycle, or test data obtained from several stabilized cycles. Stress-strain data can be obtained from several stabilized cycles of specimens that are subjected to symmetric strain cycles.

The calibration procedure consists of several cylindrical bar tests, one of which subjected to monotonic tension until necking and others were under symmetric strain-controlled experiments with different strains. During these calibration tests, the stress state must remain uniaxial.

From symmetric strain-controlled experiments, the equivalent plastic strain equals the summation of the absolute value of the change in longitudinal plastic strains:

$$\bar{\epsilon}_p = \sum_i |\Delta \epsilon_{p(i)}| = \sum_i |\Delta \epsilon_i - \Delta \bar{\sigma}_{\text{exp}} \cdot E| \quad (11)$$

where  $\epsilon_i$  total strain,  $\bar{\sigma}_{\text{exp}}$  is the measured stress and  $E$  is the elastic modulus.

The equivalent back stress,  $\bar{X}$ , equals one-half of the difference in yield stress between the end of the tensile loading and first yield of the subsequent compressive loading.

These results, corresponding  $(\bar{X}, \bar{\epsilon}_p)$  data pairs may be plotted, and the kinematic hardening parameters,  $C$  and  $\gamma$ , may be calculated by fitting Equation (10) to the data and selecting parameters minimize the sum of the square of the error between Equation (10) and the data.

For symmetric strain-controlled experiments, a typical curve with strain amplitude  $\pm 0.75$  is shown in Fig. 3. The results gained experimentally and from FE using kinematic hardening model with  $C = 3941.31 \text{ MPa}$ ,  $\gamma = 15.85$  are detailed below.

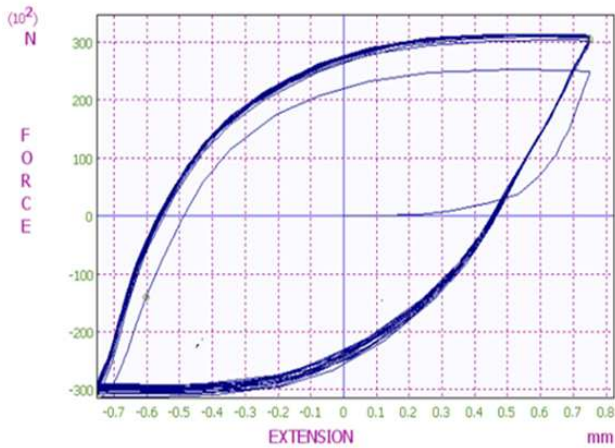


Fig 3. Typical cyclic loading curve with strain amplitude  $\pm 0.75$  for SS304 L.

Table 1. Component identification and geometry (Stainless steel) (Yahiaoui et al., 1996)

Component identification*	Thickness (mm), (schedule)	Bend Radius (mm)	Bend characteristic $H = t R/r^2$	Radius ratio $b = R/r$
SLSI	3.91, (40)	76	0.37	2.7
SLXI	5.54, (80)	76	0.56	2.8
SSSI	3.91, (40)	51	0.25	1.8
SSXI	5.54, (80)	51	0.38	1.9

\*Components are labelled by a four-character coding:  
 First character: C for carbon or S for stainless steel;  
 Second character: L for long or S for short radius bends;  
 Third character: S for standard weight or X for extra strong;  
 Fourth character: I is used here to denote in-plane bending to differentiate from another programme concerned with out-of-plane 0 Loading.

Table 2. Material (SS304) properties obtained by tensile tests (Yahiaoui et al., 1996)

Material properties				
Young's modulus	Ultimate stress	2% Proof stress	Elongation at failure (%)	$S_m = M \ln \left( \frac{1}{3} \sigma_{ult}, \frac{2}{3} \sigma_y \right)$
200GPa	597MPa	292MPa	81%	161MPa

Table 3. The frequency and Design pressure (Yahiaoui et al., 1996)

Component identification*	Frequency (Hz)	Design pressure (MPa)
SLSI	3.99	15.8
SLXI	4.11	22.8
SSSI	3.92	15.8
SSXI	4.25	22.8

## 6. Experimental and FE results

Detailed results will be presented for four of the specimens tested (SSLS, SLXI, SSSI and SSXI) and summary results will be given for all tests conducted. It is perhaps useful to present, bending moment response obtained by the FE analysis is shown in Figure. 4. Typical strain response in presence of ratchetting in FE results is shown in figure. 5.

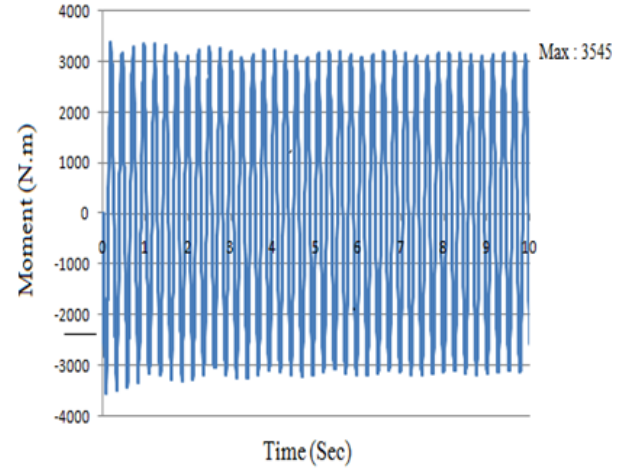


Fig 4. FE analysis dynamic bending moment responses For SSSI at a dynamic bending moment of 3546.

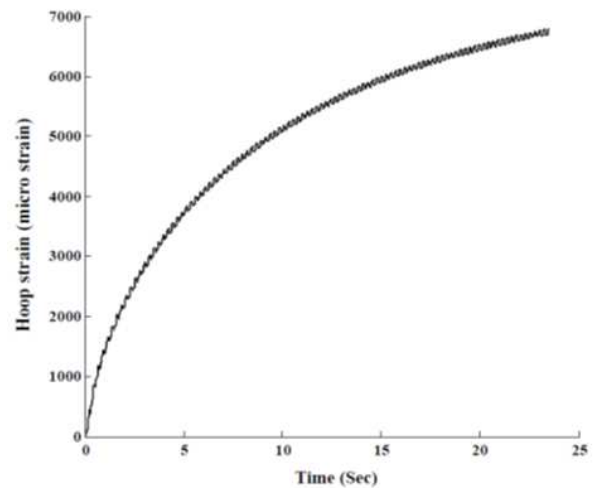


Fig 5. Typical strain response in presence of ratchetting in FE results for specimen SSSI at a dynamic bending moment of 4090 N.m.

All of the experimental ratchetting results and FE analysis on specimens SSSI, SLSI, SLXI and SSXI are plotted in Figs. 6 a, b and 7 a, b, respectively. Here, the strain for each cycle has been calculated as the average over the period of the test and plotted against  $M/M0.2$ . Figs. 6 and 7 show the data recorded for the crown surface. A typical set of results for specimen SLSI is shown in Fig. 8, which includes results from the FE analysis using with the nonlinear kinematic hardening model. Here, the ratchet strain per cycle averaged over the first 20 s of excitation has been plotted against increasing  $M/M0.2$  ratios. The same information obtained for specimens SSSI, SLXI and SSXI are illustrated in Figs. 9-11. In Table 4, the ratchet strains found experimentally over a 20 s test period and by FE analysis, for the same period, for specimen SSSI are summarized.

## 7. Results, Discussion and Conclusions

Results from tests on four pairs stainless steel some long and short radius piping elbows with two different

thicknesses have been presented. The components were subjected to steady internal pressure and resonant, dynamic in-plane bending moments. The experimental work reported here provides reliable data which can be used to judge the value of the FE analysis using the ABAQUS package. However, it should be noted that the experimental work used a rising amplitude technique which may effectively reduce the ratchet strain at any particular dynamic bending moment. It is possible that those tests conducted at low amplitude will harden the material sufficiently to reduce the ratchet strains observed at higher amplitudes. It is not possible to quantify the possible magnitude of this effect. This possible effect would not have influenced the dynamic bending moment at which ratchetting was first observed. Typical data obtained experimentally and from FE model for specimens SLXI to SSXI on the crown surface are shown in Fig. 6 and 7. The experimental and FE results illustrated by Figs 8-11 show the onset of ratchetting for stainless steel elbow specimens occur at  $0.6 \leq M / M_l \leq 0.7$  and  $0.5 \leq M / M_l \leq .75$ , respectively. Complete set of data for specimens SSSI is

presented in Table 4. In this study, Stress-strain data and material parameters have been obtained from several stabilized cycles of specimens that are subjected to symmetric strain cycles. The rate of ratchetting depends significantly on the magnitude of the internal pressure, dynamic bending moment and material constants for nonlinear kinematic hardening model. The results show that initial the rate of ratchetting is large and then it decreases with the increasing of cycles. The FE model predicts the hoop strain ratchetting rate to be greater than that found experimentally. Therefore, The results obtained from the FE method gives over estimated values comparing with the experimental data.

## Acknowledgments

Appreciation is expressed to the technical staff of the Applied Mechanics Division of the Department of Mechanical Engineering at the University of Mohaghegh Ardebili (Iran) for their assistance with the work.

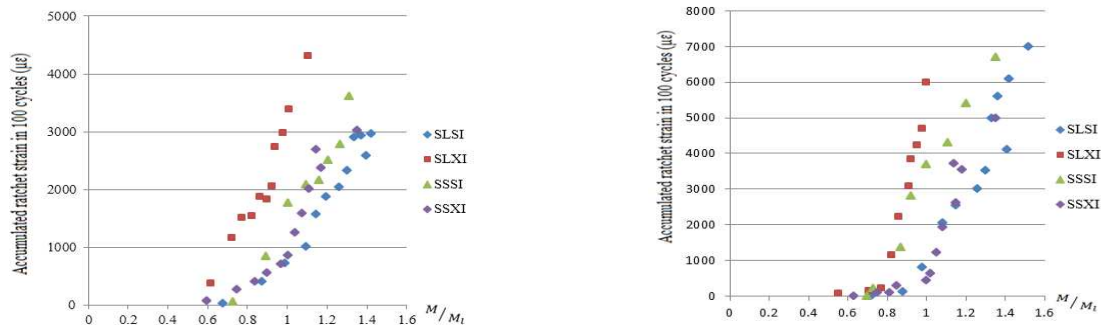


Fig 6. (a) Experimental ratchetting data (Yahiaoui et al., 1996) and (b) FE analysis against moment levels.

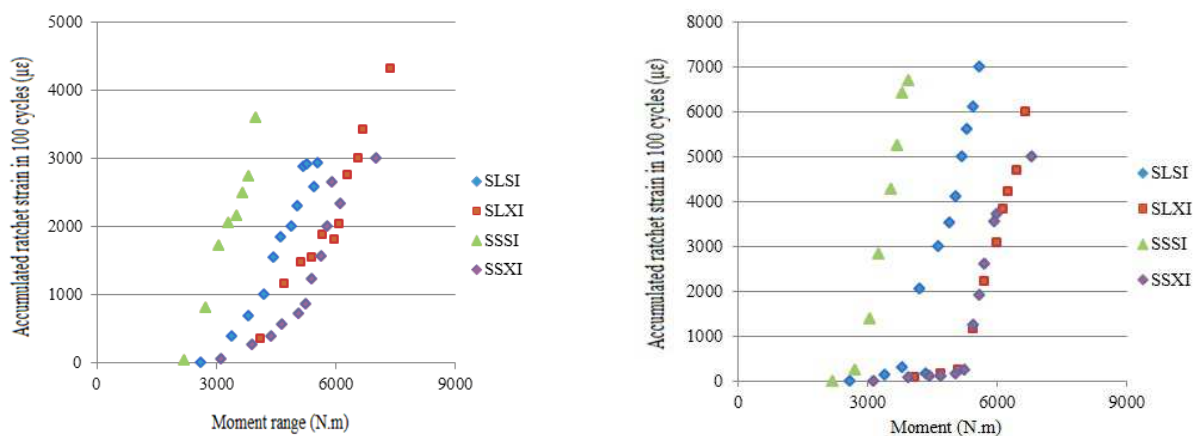


Fig 7. (a) Experimental ratchetting data (Yahiaoui et al., 1996) and (b) FE analysis against moment levels



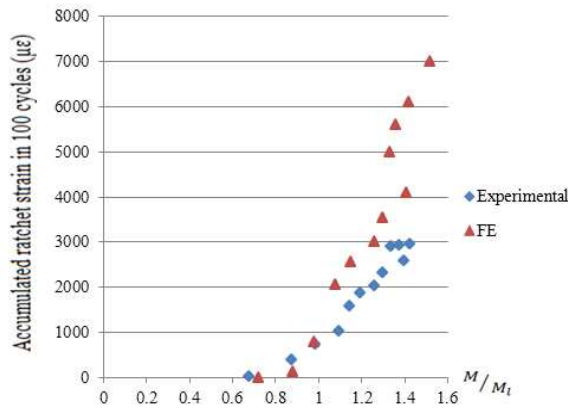


Fig 8. Experimental and FE ratchet strains(Component SLSI)

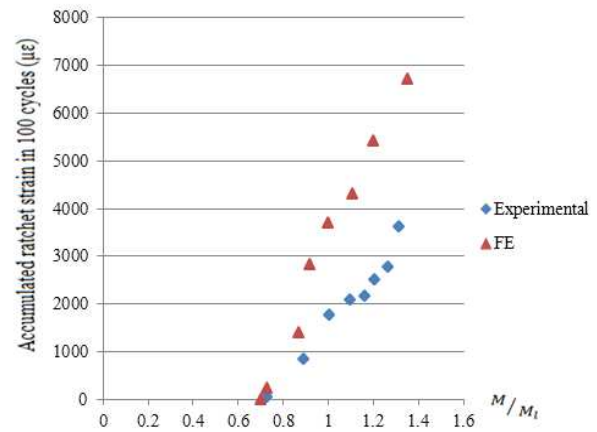


Fig 9. Experimental and FE ratchet strains(Component SSSI)

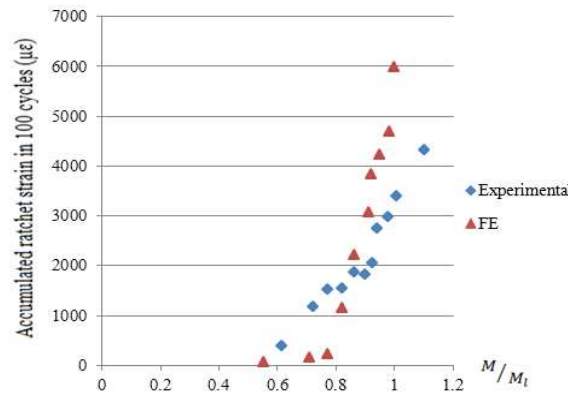


Fig 10. Experimental and FE ratchet strains(Component SLXI)

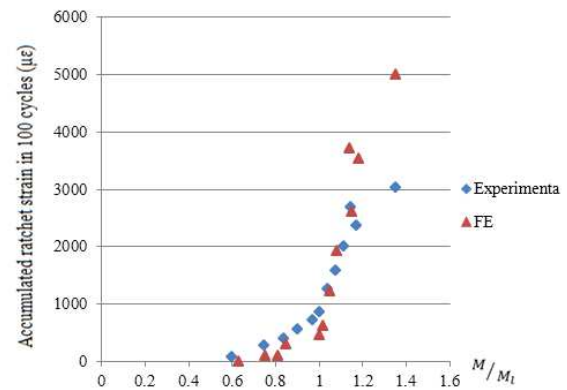


Fig 11. Experimental and FE ratchet strains(Component SSXI)

Table 4. Experimental and FE ratchetting data for specimen SSSI.

Dynamic bending moment M(N.m)	$M/M_{ye}$	$M/M_l$	Experimental ratchetting data ( $\mu\epsilon$ /cycle)	FE analysis against moment levels ( $\mu\epsilon$ /cycle)
2181	2.191	0.73	76	7
2727	2.717	0.89	769	230.51
3068	3.042	1.02	1692	1384.63
3272	3.292	1.11	2000	2815.05
3546	3.4194	1.21	2115	3319.6
3681	3.644	1.26	2461	4238.2
3818	3.794	1.3	2692	5315.9
3954	3.794	1.36	3538	6709.2
4090	3.968	1.39	4307	6801.45
4295	4.266	1.45	4851	7462.32

## Notation

$t$	Cylinder Thickness
$r$	Pipe mean radius
$E$	Young's modulus
$M$	Dynamic bending moment
$M_y$	Yield moment

$M_l$	Limit moment of elbow
$S_m$	Allowable design stress intensity
$y$	Thickness correction factor = 0.4
$\sigma_{ult}$	Tensile stress
$\sigma_y$	Yield stress
$f$	Yield surface
$h$	Bend characteristic = $tR/r^2$
$J_2$	Von-Mises yield function
$\sigma$	Stress tensor
$\sigma'$	Stress deviatoric tensor
$X$	Back stress tensor
$X'$	Back stress deviatoric tensor
$k$	Initial size of the yield surface
$C, \gamma$	Materials constants for kinematic hardening
$\epsilon^P$	Plastic strain tensor
$\epsilon_P$	Equivalent plastic strain
$\phi$	Angular position around the circumference of the bend ( $= 0^\circ$ at the crown)

## References

- [1] Abdel-Karim, M., 2005. Numerical integration method for kinematic hardening rules with partial activation of dynamic recovery term. *Int. J. of Plasticity*, 21:1303-1321.
- [2] Armstrong, P.J., Frederick, C.O., 1966. A mathematical representation of the multi axial Bauschinger effect. CEGB Report RD/B/N 731, Central Electricity Generating Board. The report is reproduced as a paper: 2007. *Materials at High Temperatures*, 24(1):1-26.
- [3] Bari, S., Hassan, T., 2000. Anatomy of coupled constitutive models for ratcheting simulation. *Int. J. of Plasticity*, 16:381-409.
- [4] Bari, S., Hassan, T., 2001. Kinematic hardening rules in uncoupled modeling for multiaxial ratcheting simulation. *Int. J. of Plasticity*, 17:885-905.
- [5] Bari, S., Hassan, T., 2002. An advancement in cyclic plasticity modeling for multiaxial ratcheting simulation. *Int. J. of Plasticity*, 18:873-894.
- [6] Chaboche, J.L., 1986. Time-independent constitutive theories for cyclic plasticity. *Int. J. of Plasticity*, 2: 149-188.
- [7] Chaboche, J.L., 1991. On some modifications of kinematic hardening to improve the description of ratcheting effects. *Int. J. of Plasticity*, 7:661-678.
- [8] Chaboche, J.L., 2008. A review of some plasticity and viscoplasticity constitutive theories, *Int. J. of Plasticity*, 24:1642-1963
- [9] Chen X, Gao B, Chen G, 2005. Multiaxial ratcheting of pressurized elbows subjected to reversed in-plane bending. *J Pres Eq Syst*;3:38-44.
- [10] Chen X, Gao B, Chen G, 2006. Ratcheting study of pressurized elbows subjected to reversed in-plane bending. *J Pres Ves-Trans ASME*;128:525-32.
- [11] Chen, Xiaohui., Chen, Xu., Yu, Dunji., Gao, Bingjun., 2013. Recent progresses in experimental investigation and finite element analysis of ratcheting in pressurized piping, *Int. J. of Pressure Vessels and Piping* , 101:113-142.
- [12] Lemaitre, J and Chaboche, J.L., 1994. *Mechanics of Solid Materials*, Published by Cambridge University Press, ISBN 0521477581, 9780521477581, 584 pages.
- [13] Mahbadi, H. and Eslami, M.R., 2006. Cyclic loading of thick vessels based on the Prager and Armstrong-Frederick kinematic hardening models. *Int. J. of Pressure Vessels and Piping*, 83:409-419
- [14] Ohno, N., Wang, J.D., 1993. Kinematic hardening rules with critical state of dynamic recovery, part I: formulations and basic features for ratcheting behavior. *J. of Plasticity*, 9: 375-390.
- [15] Rahman, S.M., Hassan, T., Corona, E., 2008. Evaluation of cyclic plasticity models in ratcheting simulation of straight pipes under cyclic bending and steady internal pressure. *Int. J. of Plasticity*, 24:1756-1791.
- [16] Tasnim, H., Kyriakides, S., 1992. Ratcheting in cyclic Plasticity, part I: uniaxial behavior. *Int. J. of Plasticity*, 8:91-116.
- [17] Tasnim, H., Corona, E., Kyriakides, S., 1992. Ratcheting in cyclic plasticity, part II: multiaxial behavior. *Int. J. of Plasticity*, 8: 117-146
- [18] Tasnim, H., Lakhdar, T., Shree, K., 2008. Influence of non-proportional loading on ratcheting responses and simulations by two recent cyclic plasticity models, *Int. J. of Plasticity*, (24) 1863-1889.
- [19] Yahiaoui, K., Moffat, D.G., Moreton, D.N., 1996. Response and cyclic strain accumulation of pressurized piping elbows under dynamic in plane bending, *J. of strain analysis* vol 31 No 2.
- [20] Zakavi, S.J., Zehsaz, M., Eslami, M.R. (2010) The ratchetting behavior of pressurized plain pipework subjected to cyclic bending moment with the combined hardening model. *Nuclear Engineering and Design*, 240(4), 726-737.